Svedberg Open
DISSEMINATION OF KNOWLEDGE

International Journal of Artificial Intelligence and Machine Learning

Publisher's Home Page: https://www.svedbergopen.com/

Research Paper Open Access

Integrating Ca-Scl Polar Decoding With Noma and Sic For Reliable Mmtc in 5g Networks

K.Chandra Sekhar[1], G.Sateesh Kumar[2], B.T.Krishna[3]

[1]Research Scholar, Dept. of Ece, University College of Engineering, JNTU-K, Kakinada, AP, India. Email: csk925@gmail.com
[2]Professor, Dept. of Ece, Aditya Institute of Technology & Management, Tekkali, AP, India.
[3]Professor, Dept. of Ece, University College of Engineering, JNTU-K, Kakinada, AP, India.

ABSTRACT
5G's massive machine-type communication (mMTC) requires networks to support a huge number of devices with stringent reliability and delay requirements. The 5G New Radio (NR) standard now includes polar codes, which are ideal for these kinds of situations, especially when decoded using algorithms called Cyclic Redundancy Check (CRC)-aided Successive Cancellation List (CA-SCL). Non-Orthogonal Multiple Access (NOMA) combined with Successive Interference Cancellation (SIC) has been found to be an effective method on a large scale. This paper aims to improve the reliability of CA-SCL polar decoding by combining it with NOMA and SIC. The Results are compared with traditional coding Techniques like LDPC and Turbo and it is observed that the Proposed Technique provides a better performance and Trade-off especially at low SNR's.

Keywords: CA-SCL, Polar Codes, mMTC, NOMA, SIC, 5G NR

Introduction

Polar codes, which are introduced as a capacity-achieving family of error correction codes, have been adopted in the 5G New Radio (NR) standard for control channels. Their performance can be further improved through Cyclic Redundancy Check (CRC)-aided Successive Cancellation List (CA-SCL) decoding, which balances reliability with manageable decoding complexity. However, most prior research on polar decoding has focused on single-user links under simple channel conditions, leaving open questions about its effectiveness in multi-user mMTC scenarios.

In parallel, Non-Orthogonal Multiple Access (NOMA) has been proposed to increase spectral efficiency by allowing multiple users to share the same resources, while Successive Interference Cancellation (SIC) is employed to separate overlapping signals at the receiver. By combining CA-SCL polar decoding with NOMA and SIC, it becomes possible to address both coding and access challenges in mMTC, offering an integrated approach to reliability and scalability.

Literature Study

Polar codes were introduced by Arıkan [1] as the first provably capacity-achieving codes for binary-input memoryless channels. Successive cancellation (SC) decoding offers low complexity but limited error resilience at short block lengths. Tal and Vardy [2] improved this using successive cancellation list (SCL) decoding, while Niu and Chen [3] enhanced it with CRC-aided list decoding (CA-SCL), which became the practical choice for 5G NR control channels [8]. Numerous extensions have been proposed: adaptive list-size selection [4], partitioned SCL (PSCL) [5], fast/SSC-based decoding [6], LLR-domain implementations [7], and hardware-oriented designs [24], [25], [26], [27]. These contributions address latency, memory, and energy bottlenecks, demonstrating that CA-SCL polar decoders can meet the demands of short-packet ultra-reliable communication in IoT and vehicular systems [22], [23].

Parallel advances in multiple access identified non-orthogonal multiple access (NOMA) as a spectrum-efficient solution for 5G and beyond. Ding et al. [9] and Dai et al. [10] highlighted its benefits in spectral efficiency and fairness, while Islam et al. [11] and Ye et al. [12] discussed uplink design challenges such as power control and SIC error propagation. Choi [28] and Sun et al. [29] optimized power allocation and user pairing to stabilize SIC. For massive machine-type communication (mMTC), where devices generate short and sporadic traffic, Bockelmann et al. [14] set out physical/MAC solutions, and Shahab et al. [13] provided a comprehensive survey of grant-free NOMA access. Further, Gao et al. [15] and Liu et al. [16] demonstrated compressive-sensing and outage analysis frameworks for grant-free connectivity. Liu et al. [30] positioned NOMA as a scalable solution for IoT access, emphasizing that SIC remains a viable receiver strategy for high-density deployments.

Recent research combines these two fronts by integrating polar coding with NOMA and SIC. Dai et al. [17] introduced polar-coded NOMA (PC-NOMA), aligning polarization with superimposed channels, while Marshakov et al. [18] studied polar codes over Gaussian MAC and polar-coded NOMA. Ebada et al. [19] investigated iterative detection and decoding of finite-length polar codes in multiuser channels. Xie et al. [20] combined polar coding with physical network coding to enhance downlink NOMA fairness, and Cui et al. [21] proposed intelligent path-selection-aided CA-SCL decoding for reduced complexity. Hybrid SC-list decoding [22] and low-latency architectures [23] strengthen polar decoders for IoT. Additional innovations such as fast SSC-Flip decoding [25] and energy-efficient hardware [27] confirm the feasibility of deploying CA-SCL in practical systems. Collectively, these works illustrate the potential of joint coding–multiple access strategies. However, most studies consider coding or access in isolation. A holistic evaluation of CA-SCL polar decoding under NOMA/SIC in realistic mMTC conditions—covering BER, FER, collision rates, latency, throughput, and energy per bit—remains limited, which motivates the present study.

Proposed work

The proposed work provides an end-to-end uplink mMTC simulation framework that starts with system initialization, where key parameters such as modulation formats, list sizes, SNR ranges, traffic intensity, and channel conditions are configured, and proceeds through nested loops to assess multiple operating scenarios. In each frame, device activity is generated using a Poisson process, and active users are assigned to slots, capturing the effects of contention and potential collisions. User data is then processed by appending CRC bits, followed by polar encoding and modulation, before being transmitted through a NOMA channel modeled under AWGN or Rayleigh fading conditions. At the receiver, successive interference cancellation (SIC) combined with CRC-aided polar list decoding is employed to iteratively recover user signals and improve decoding reliability. System performance is evaluated by calculating metrics such as BER, FER, collision rate, packet and access success probabilities, throughput per user, latency, and energy per bit. The strength of the proposed work lies in its integrated evaluation of traffic variability, channel coding, multi-user access, and decoding mechanisms, enabling a realistic analysis of trade-offs among reliability, spectrum efficiency, latency, and energy consumption, thereby serving as an effective tool for optimizing next-generation 5G/6G IoT systems.

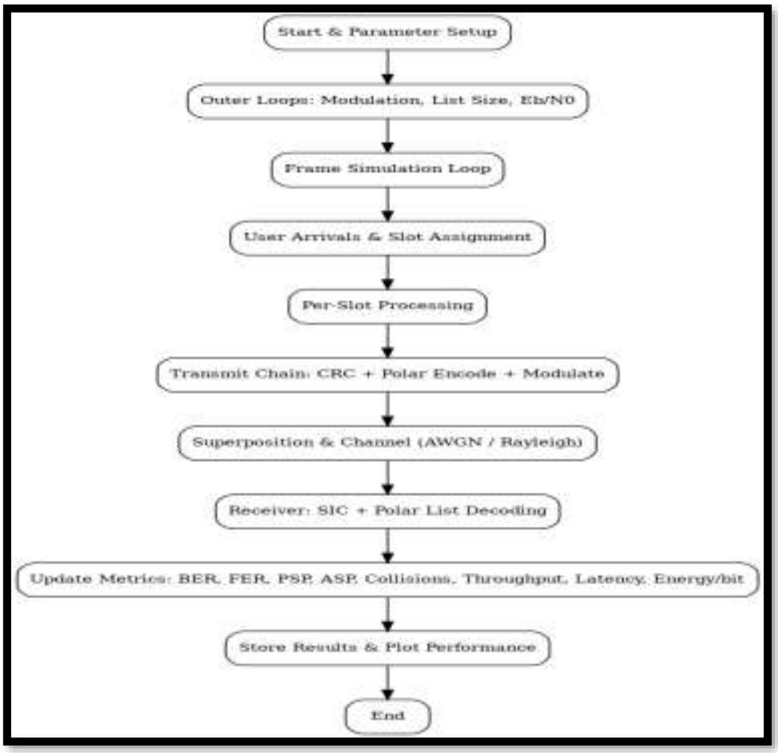

Figure 1 : Flow Chart of the Proposed Work

Mathematical Modelling

Step 1: Input Message Bits

The Transmitted message for each device is represented as a sequence of independent binary bits $u=[u0,u1,\ldots,u_{K-1}]\in\{0,1\}^{Km}$ ----------(i) ; where K_m is the number of information bits.

Step 2: CRC Appending

To improve error detection and enable list decoding, a set of CRC (Cyclic Redundancy Check) bits are appended to the original message. Compute a parity sequence of length L_{CRC} using a generator polynomial g(D) such that $p=CRC(u,g(D))\in\{0,1\}^{L_{CRC}}$ ---------- (ii)

The combined block is $d=[u,p]\in\{0,1\}^K$,$K=K_m+L_{CRC}$ -----------(iii)

Step 3: Polar Encoding

Polar codes rely on channel polarization after applying the polar transform, some bit positions become highly reliable, while others become very unreliable . Indices where bits are reliable carry actual data and they are chosen from Information set I, where as indices where bits are unreliable are fixed to a known value (usually 0) and they are chosen from Frozen set F. The encoder input vector is

$$a_i = \begin{cases} d_j, & i \in \mathcal{I} \quad \text{(information bits)} \\ 0, & i \in \mathcal{F} \quad \text{(frozen bits)} \end{cases} \text{-------------- (iv)}$$

$c=d\cdot G_N$, where $G_N = F\otimes n$ --------(v) where ,$N=2^n$ & $F=\begin{bmatrix}1 & 0\\ 1 & 1\end{bmatrix}$ and $\otimes n$ is the n-fold Kronecker product.

Step 4 : Rate matching

To ensure the code fits the required Transmission Rate and length we perform puncturing/shortening, the final code word length is now given by

$b \in\{0,1\}Eeff$, $R=K/Eeff$. --------- (vi)

Step 5 : Bit to Symbol Mapping/ Modulation

Group bits into log2 M tuples and map to constellation points

$s_n = \mu(b_n)$, $s_n \in S^M$, where $n = 1 , \ldots Eeff / \log_2 M$ --------------(vii)

Step 6 : Slot Assignment and Arrivals

The number of users requesting access in each frame is modelled as $A\sim$ Poisson(λ) which is given by

$$\Pr(A = a) = \frac{\lambda^a e^{-\lambda}}{a!}, \quad a = 0,1,2, \ldots \text{-------------(viii)}$$

This captures the random and independent nature of device activity. We start with S slots (like S "bins" where users can go). At the beginning, all are empty

$O_s = 0, \quad s = 1,2, \ldots , S$ ----------(ix)

Here O_s = number of users already in slot s. Since no one has arrived yet, every slot has zero users. When a new user u arrives, they need to be placed into a slot. The system looks at all slots and chooses the one with the least number of users given by

$$s_u = \arg\min_{s\in\{1,\ldots,S\}} O_s \text{ ------------(x)}$$

Once the slot is chosen, we update the occupancy counter

$O_{s_u} \leftarrow O_{s_u} + 1$ -----------(xi)

Each slot can only handle up to U_{max} users safely. If more users are placed into a slot, the extra ones cause a collision. For each slot the Collisions are given by

Collisions in slot $s = \max(O_s - U_{max}, 0)$ ----------(xii)

If $O_s \leq U_{max}$, no collision occurs (value is 0) ; If $O_s > U_{max}$, the extra users are counted as collisions.

Total collisions across all slots is given by

$C = \sum_{s=1}^{S} \max (O_s - U_{max}, 0)$ ----------(xiii)

Step 7: NOMA Power Allocation

This scheme assigns decreasing power levels to successive users according to a geometric decay factor $(1-\alpha)$. After normalization, all users' power fractions sum to one. The idea is that the first user in the decoding order gets the largest share of power, and each subsequent user gets less. This matches the successive interference cancellation (SIC) decoding order: strong users with good channels are allocated less power but can still decode reliably, while weaker users are given more power to improve their chances of successful reception. All the Powers are Normalized as per the following equation

$$P_k = \frac{P_{tot}(1-\alpha)^{k-1}}{\sum_{j=1}^{U}(1-\alpha)^{j-1}}, \quad k = 1,2, \ldots , U \text{ -------------(xiv)}$$

The Transmitted Super imposed NOMA Signal is now given by

$x = \sum_{k=1}^{U} \sqrt{P_k}\, s_k$ ------------ (xv)

Step 8 : Channel Transmission

Once the superimposed NOMA signal is generated, it is transmitted through either an AWGN or Rayleigh fading channel. In the AWGN case, the signal is only affected by Gaussian noise, while in the Rayleigh case, the signal first undergoes amplitude and phase distortion due to fading and then is corrupted by Gaussian noise. This formulation captures realistic wireless propagation effects before SIC-based decoding is applied at the receiver.

AWGN Modelling

$r_n = x_n + w_n, \quad w_n \sim \mathcal{CN}(0, \sigma^2)$. -----------(xvi)

Rayleigh Fading $h_{slot} = 1/U \sum_k h_k$ -------------(xvii)

$r = h_{slot} x + w, \quad w \sim \mathcal{CN}(0, \sigma^2)$. -------------(xviii)

Step 9: Equalization

once the NOMA signal is received, it undergoes equalization to counteract the channel distortion. This is achieved by dividing the received signal by the channel coefficient, thereby restoring the transmitted waveform.

$y = r/h_{slot} = x + \tilde{w}$, ---------(xix) where $\tilde{w} = w/h_{slot}$ & $\tilde{w} \sim \mathcal{CN}(0, \sigma^2/|h_{slot}|^2)$.

After equalization, the noise power is scaled by the channel gain.

$\sigma_{eff}^2 = \sigma^2/|h_{slot}|^2$. -------------(xx)

Step 10: LLR Decoding

Once the signal is equalized and the effective noise variance is obtained, the receiver computes log-likelihood ratios (LLRs) for each transmitted bit. The LLR provides a measure of confidence about whether a bit is more likely to be a 0 or a 1, based on the Euclidean distance between the received symbol and the possible constellation points, scaled by the effective noise level. These soft values are essential for polar decoding, since they provide richer reliability information than hard decisions, significantly improving error correction performance.

$L_m(y) = \log \frac{\Pr(b_m=0|y)}{\Pr(b_m=1|y)}$. ----------(xxi)

Step 11 : Integrating SIC& LLR

After equalization and noise adjustment, the receiver evaluates log-likelihood ratios (LLRs) for each transmitted bit. For a received symbol yeq, the LLR corresponding to bit position b is calculated as:

$$L_m(y) = \log \frac{\sum_{s \in S_m^0} \exp(-|y-s|^2/\sigma_{eff}^2)}{\sum_{s \in S_m^1} \exp(-|y-s|^2/\sigma_{eff}^2)} \quad \text{----------(xxii)}$$

If multiple users' symbols are superimposed with power weights √Pi, then

$$L_m(y) = \log \frac{\sum_{s \in S_m^0} \exp\left(-\frac{|y-\sum_i \sqrt{P_i} s_i|^2}{\sigma_{eff}^2}\right)}{\sum_{s \in S_m^1} \exp\left(-\frac{|y-\sum_i \sqrt{P_i} s_i|^2}{\sigma_{eff}^2}\right)}. \quad \text{------------(xxiii)}$$

After cancelling stronger users in SIC, the residual looks like a single-user signal so it simplifies to

$$L_m(y) \approx \log \frac{\sum_{s \in S_m^0} \exp\left(-\frac{|y-s|^2}{\sigma_{eff}^2}\right)}{\sum_{s \in S_m^1} \exp\left(-\frac{|y-s|^2}{\sigma_{eff}^2}\right)} \quad \text{----------(xxiv)}$$

If decoding is successful, the estimated signal of user k is reconstructed:

$\hat{x}_k = \text{Modulate}\left(\text{Rate Match}\left(\text{Polar Encode}([\hat{b}_k, \text{CRC}])\right)\right)$ -----------(xxv)

Then its contribution is subtracted from the residual and it is given by

$r_{residual} \leftarrow r_{residual} - \sqrt{P_k}\, h\, \hat{x}_k$ -------------(xxvi)

Results and Discussions

Bit Error Rate : Ratio of incorrectly decoded information bits to the total transmitted information bits. The Values for different Modulation Techniques with Varying List Sizes are Tabulated below

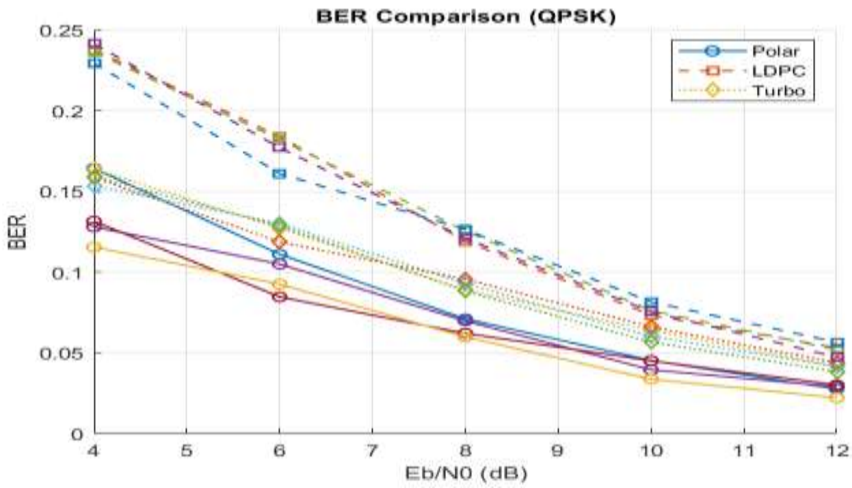

Figure 2 : Simulation Result for BER vs Eb/NO (db)

The above figure shows simulation Result for Bit error Rate and the Increasing list size reduces errors across all SNR values, Larger lists (L=4, L=8) achieve the best error performance, highlighting the trade-off between decoding complexity and reliability.

Frame Error Rate : Ratio of erroneous frames to the total number of transmitted frames. A frame is in error if at least one bit is incorrect. The Values for different Modulation Techniques with Varying List Sizes are Tabulated below

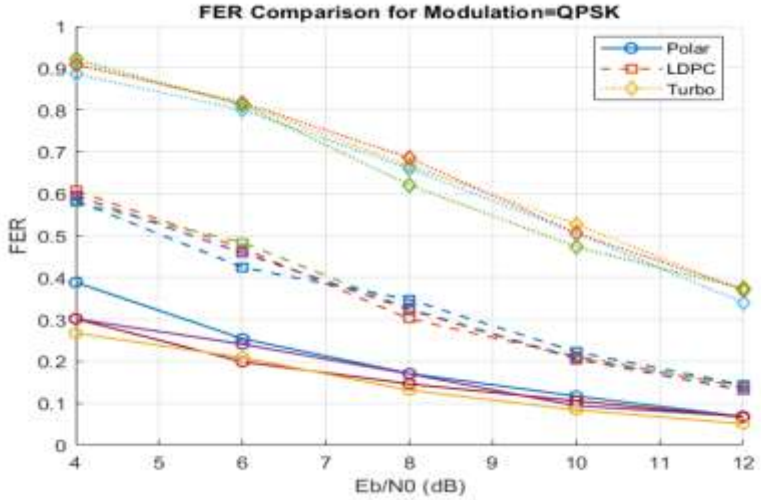

Figure 3 : Simulation Result for FER vs Eb/NO (db)

The above plot shows the Frame Error Rate (FER) versus Eb/N0 for QPSK under different list sizes. As expected, FER decreases with increasing SNR, since higher Eb/N0 improves decoding reliability. Among the schemes, Polar Codes consistently achieves lower FER , reflecting its greater robustness to noise. Additionally, larger list sizes (L=4, L=8) significantly reduce FER compared to smaller lists, as more decoding paths are explored, which increases the chances of recovering the correct codeword. At low SNR, errors remain high across all cases, but with sufficient SNR (above ~2 dB), the advantage of larger lists becomes clear, highlighting their effectiveness in enhancing system reliability.

Latency : Average time consumed in decoding per successfully received packet. The below figure presents the latency per successful packet versus Eb/N0 for QPSK across different list sizes. The results indicate that latency remains relatively stable across SNR values, with only minor fluctuations. QPSK with smaller list sizes shows slightly higher latency at low Eb/N0 due to increased decoding effort, whereas larger list sizes maintain more consistent performance. Overall, the graph highlights that while decoding complexity and modulation type affect latency, the variations are small, suggesting the system can achieve low-delay communication suitable for mMTC applications.

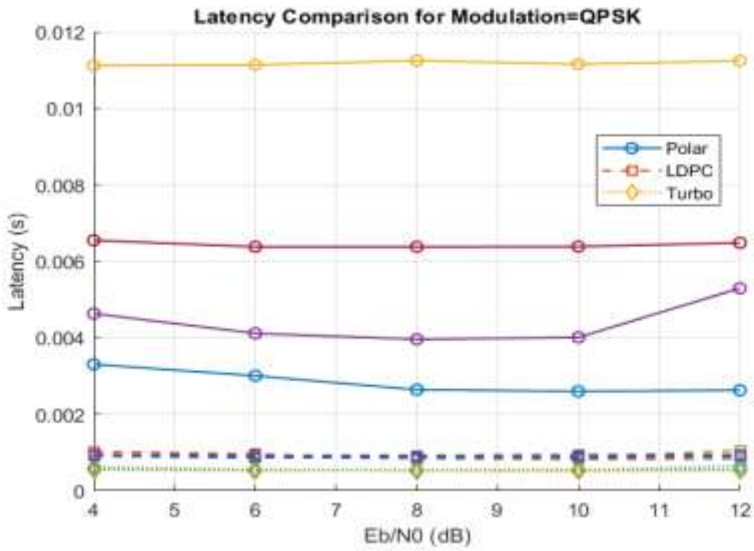

Figure 4 : Simulation Result for Latency vs Eb/NO (db)

Packet Success Probability & Access Success Probability : Probability that an arriving packet is decoded correctly without error is called Packet Success Probability and Ratio of the number of users that were successfully decoded to the number of arrivals is called Access Success Probability and the Values are tabulated below.

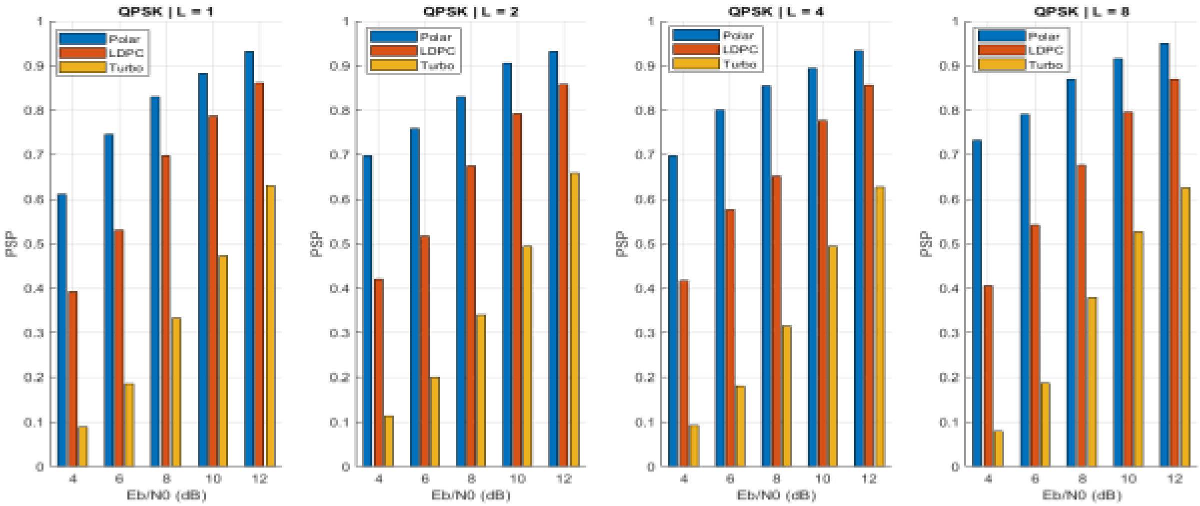

Figure 5 : Simulation Result for PSP vs Eb/NO (db)

The above figure shows the Packet Success Probability (PSP) and Access Success Probability (ASP) versus Eb/N0 for QPSK with different list sizes is shown below. Both metrics improve as Eb/N0 increases, reflecting better reliability in higher SNR conditions. Polar Codes generally achieves higher PSP and ASP compared to other Coding Techniques, showing its robustness in low-SNR regimes. Larger list sizes also enhance performance, since more decoding paths increase the chance of recovering the correct codeword. However, the improvement is more noticeable at higher Eb/N0 values, where decoding benefits from reduced noise interference.

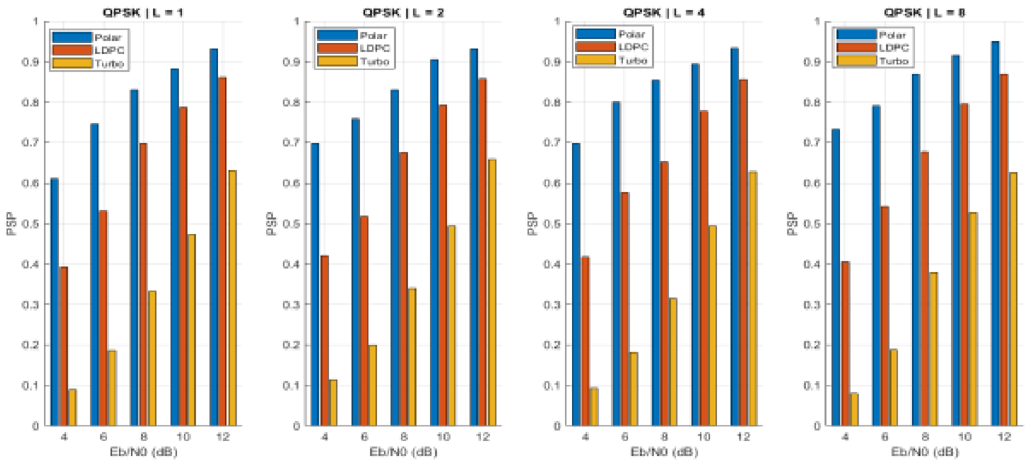

Figure 6: Simulation Result for ASP vs Eb/NO (db)

Throughput : Average correctly decoded information bits per arrival, normalized by the code length. The below figure illustrates the throughput per user versus Eb/N0 for QPSK across different list sizes. The results show that throughput increases as Eb/N0 rises, since higher signal quality leads to more successful packet decoding. Polar Codes generally achieves higher throughput compared to other techniques, particularly at lower SNR values, reflecting its robustness in noisy conditions. Overall, the graph highlights the trade-off between modulation type, decoding complexity, and channel quality in determining user throughput in mMTC systems.

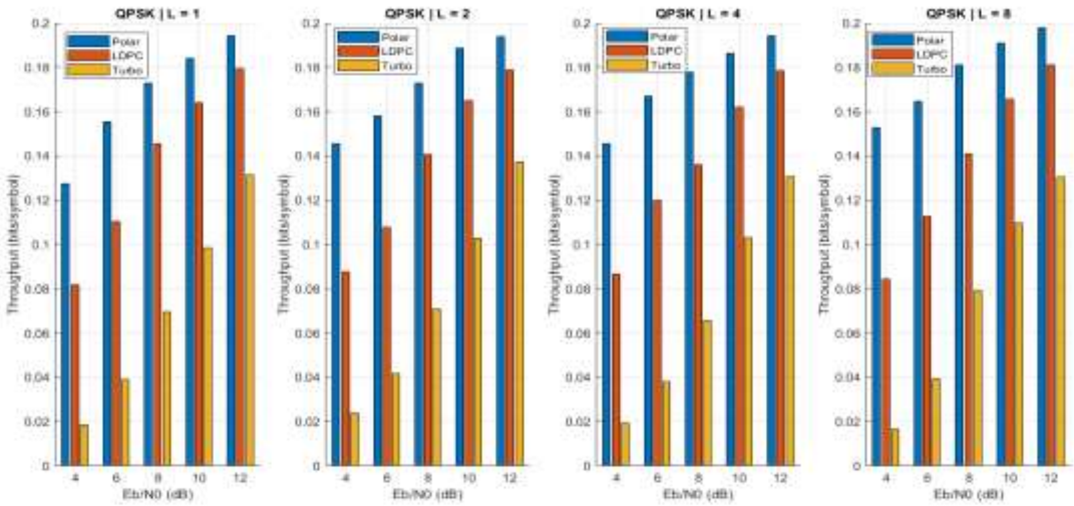

Figure 7 : Simulation Result for Throughput per user vs Eb/NO (db)

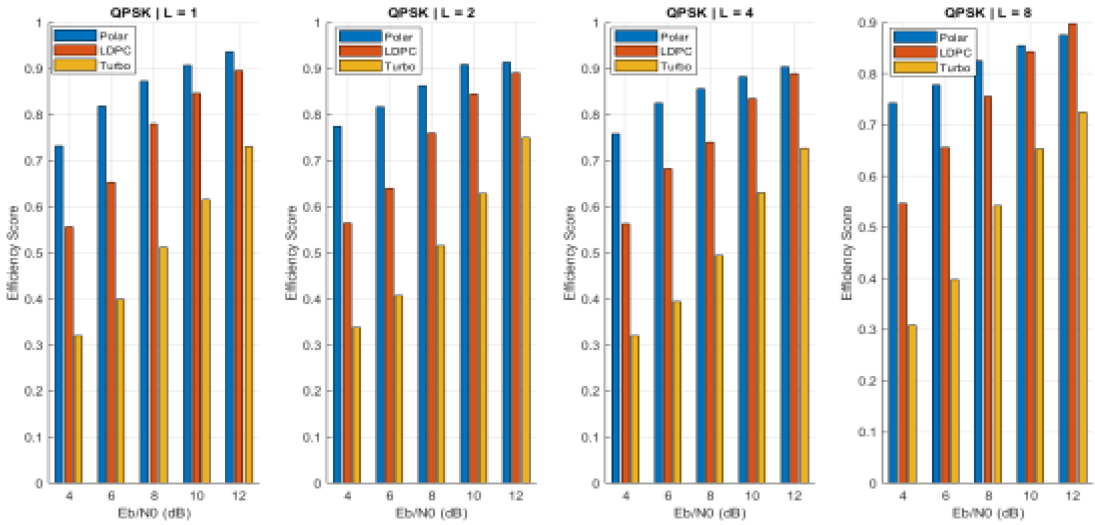

Figure 8 : Efficiency Score for Polar, LDPC, Turbo at different List Sizes.

Finally efficiency score is calculated for all the coding techniques with parameters such as Bit Error Rate (BER), Frame Error Rate (FER), Arrival Success Probability (ASP) , Packet Success Probability (PSP), Throughput and Latency. Among all the three coding Techniques Polar Codes are found to be efficient when compared to LDPC and Turbo Codes and also provide better Trade off for Mmtc Applications. However their latency increases as SNR and List size Increases. The Efficiency Score Values are listed below.

Table 1 : Comparison of Efficiency score for Polar, LDPC & Turbo for List Sizes L=1,2

Sno	Eb/No	List Length (L=1)			List Length (L=2)		
		POLAR	LDPC	TURBO	POLAR	LDPC	TURBO
1	4	0.7331	0.5551	0.3198	0.7791	0.5654	0.3390
2	6	0.8180	0.6530	0.3980	0.8150	0.6406	0.4072
3	8	0.8731	0.7804	0.5122	0.8626	0.7607	0.5165
4	10	0.9072	0.8460	0.6156	0.9095	0.8446	0.6299
5	12	0.9370	0.8952	0.7314	0.9249	0.8929	0.7518

Table 2 : Comparison of Efficiency score for Polar, LDPC & Turbo for List Sizes L=4,8

Sno	Eb/No	List Length (L=4)			List Length (L=8)		
		POLAR	LDPC	TURBO	POLAR	LDPC	TURBO
1	4	0.7606	0.5638	0.3207	0.7420	0.5462	0.3086
2	6	0.8252	0.6841	0.3937	0.7757	0.6553	0.3970
3	8	0.8576	0.7402	0.4948	0.8266	0.7560	0.5430
4	10	0.8830	0.8345	0.6303	0.8568	0.8438	0.6529

5	12	0.9064	0.8900	0.7277	0.8776	0.8981	0.7254

Conclusion

In this Proposed work, CRC-aided successive cancellation list (CA-SCL) polar decoding is combined with successive interference cancellation (SIC) and non-orthogonal multiple access (NOMA) in massive machine-type communication (mMTC) scenarios. Polar codes are widely recognized for their near-capacity performance at short block lengths, and NOMA has been thoroughly investigated for its spectrum efficiency; however, there hasn't been much research done on their combined use in practical mMTC scenarios. By investigating how CA-SCL decoding can lessen the reliability issues associated with short-packet transmissions in high-density settings, while NOMA and SIC handle scalability and spectrum sharing, this study advances the field.

It provides a balanced trade-off between reliability and latency, as CA-SCL enhances error performance without excessive overhead. Second, coupling polar decoding with NOMA/SIC enables efficient spectrum reuse, allowing multiple devices to transmit simultaneously without prohibitive collision rates. Third, the approach inherently supports scalability, as the combination can sustain dense connectivity while maintaining throughput and energy efficiency. Finally, by analyzing performance metrics such as error rates, throughput per user, latency, and energy per bit, this study establishes a comprehensive framework that highlights both the coding-level and system-level advantages of the proposed integration. The proposed approach addresses critical challenges of mMTC—namely, reliability, collision management, and scalability—making it a promising solution for 5G and beyond (6G) applications.

References

[1] E. Arıkan, "Channel polarization: A method for constructing capacity-achieving codes for symmetric binary-input memoryless channels," IEEE Trans. Inf. Theory, vol. 55, no. 7, pp. 3051–3073, Jul. 2009, doi: 10.1109/TIT.2009.2021379.

[2] I. Tal and A. Vardy, "List decoding of polar codes," IEEE Trans. Inf. Theory, vol. 61, no. 5, pp. 2213–2226, May 2015, doi: 10.1109/TIT.2015.2404214.

[3] K. Niu and K. Chen, "CRC-aided decoding of polar codes," IEEE Commun. Lett., vol. 16, no. 10, pp. 1668–1671, Oct. 2012, doi: 10.1109/LCOMM.2012.081312.121204.

[4] B. Li, H. Shen, and D. Tse, "An adaptive successive cancellation list decoder for polar codes with CRC," IEEE Commun. Lett., vol. 16, no. 12, pp. 2044–2047, Dec. 2012, doi: 10.1109/LCOMM.2012.100912.121583.

[5] S. A. Hashemi, A. Balatsoukas-Stimming, P. Giard, C. Thibeault, and W. J. Gross, "Partitioned successive-cancellation list decoding of polar codes," IEEE Trans. Signal Process., vol. 65, no. 2, pp. 504–518, Jan. 2017, doi: 10.1109/TSP.2016.2626279.

[6] G. Sarkis, P. Giard, A. Vardy, C. Thibeault, and W. J. Gross, "Fast polar decoders: Algorithm and implementation," IEEE J. Sel. Areas Commun., vol. 32, no. 5, pp. 946–957, May 2014, doi: 10.1109/JSAC.2014.140520.

[7] A. Balatsoukas-Stimming, A. Raymond, W. J. Gross, and A. Burg, "LLR-based successive cancellation list decoding of polar codes," IEEE Trans. Signal Process., vol. 63, no. 19, pp. 5165–5179, Oct. 2015, doi: 10.1109/TSP.2015.2442920.

[8] 3GPP, "NR; Multiplexing and channel coding," 3GPP TS 38.212, Rel. 15–18, 2022.

[9] Z. Ding, Y. Liu, J. Choi, Q. Sun, M. Elkashlan, and H. V. Poor, "Application of non-orthogonal multiple access in LTE and 5G networks," IEEE Commun. Mag., vol. 55, no. 2, pp. 185–191, Feb. 2017, doi: 10.1109/MCOM.2017.1500657CM.

[10] L. Dai, B. Wang, Z. Ding, Z. Wang, S. Chen, and L. Hanzo, "A survey of non-orthogonal multiple access for 5G," IEEE Commun. Surveys Tuts., vol. 20, no. 3, pp. 2294–2323, 3rd Quart. 2018, doi: 10.1109/COMST.2018.2835558.

[11] S. M. R. Islam, N. Avazov, O. A. Dobre, and K.-S. Kwak, "Power-domain non-orthogonal multiple access (NOMA) in 5G systems: Potentials and challenges," IEEE Commun. Surveys Tuts., vol. 19, no. 2, pp. 721–742, 2nd Quart. 2017, doi: 10.1109/COMST.2016.2621116.

[12] N. Ye, X. Li, H. Yu, W. Liu, and X. Hou, "Uplink non-orthogonal multiple access: A survey," IEEE Wireless Commun., vol. 25, no. 2, pp. 1–7, Apr. 2018, doi: 10.1109/MWC.2018.1700274.

[13] M. B. Shahab, R. Abbas, M. Shirvanimoghaddam, W. Hardjawana, Y. Li, and B. Vucetic, "Grant-free non-orthogonal multiple access for IoT: A survey," IEEE Commun. Surveys Tuts., vol. 22, no. 3, pp. 1805–1838, 3rd Quart. 2020, doi: 10.1109/COMST.2020.2966995.

[14] G. Bockelmann et al., "Massive machine-type communications in 5G: Physical and MAC-layer solutions," IEEE Commun. Mag., vol. 54, no. 9, pp. 59–65, Sep. 2016, doi: 10.1109/MCOM.2016.7565189.

[15] Z. Gao, L. Dai, Z. Wang, S. Chen, and L. Hanzo, "Compressive sensing-based grant-free massive access for 6G," IEEE J. Sel. Areas Commun., vol. 39, no. 3, pp. 759–776, Mar. 2021, doi: 10.1109/JSAC.2021.3052484.

[16] Y. Liu, Z. Qin, M. Elkashlan, Y. Gao, and L. Hanzo, "Grant-free NOMA for massive IoT: Outage probability

and throughput," IEEE Trans. Commun., vol. 68, no. 8, pp. 4747–4761, Aug. 2020, doi: 10.1109/TCOMM.2020.2990242.
[17] J. Dai, K. Niu, Z. Si, C. Dong, and J. Lin, "Polar-coded non-orthogonal multiple access," IEEE Trans. Signal Process., vol. 66, no. 6, pp. 1374–1388, Mar. 2018, doi: 10.1109/TSP.2017.2784124.
[18] E. Marshakov, A. Miloslavskaya, and V. Miloslavskaya, "Design and decoding of polar codes for the Gaussian MAC and polar-coded NOMA," in Proc. IEEE ISIT, Paris, France, 2019, pp. 1157–1161, doi: 10.1109/ISIT.2019.8849398.
[19] M. Ebada, H. V. Poor, and L. Lampe, "Iterative detection and decoding of finite-length polar codes in Gaussian multiple access channels," IEEE Trans. Commun., vol. 68, no. 11, pp. 6915–6929, Nov. 2020, doi: 10.1109/TCOMM.2020.3016072.
[20] Z. Xie, P. Chen, and Y. Li, "Joint polar coding and physical network coding for downlink NOMA," IEEE Access, vol. 11, pp. 32684–32693, 2023, doi: 10.1109/ACCESS.2023.3261349.
[21] H. Cui, S. Wu, X. Dai, and X. You, "Intelligent path-selection-aided decoding of polar codes," IEEE Trans. Commun., vol. 71, no. 5, pp. 2271–2284, May 2023, doi: 10.1109/TCOMM.2023.3244522.
[22] J. Dai, K. Niu, and J. Lin, "Hybrid SC-list decoding of polar codes for low-latency IoT applications," IEEE Access, vol. 9, pp. 118055–118066, 2021, doi: 10.1109/ACCESS.2021.3106939.
[23] H. Li, C. Zhang, and Y. Liu, "Low-latency polar decoders for massive IoT devices," IEEE Trans. Veh. Technol., vol. 70, no. 7, pp. 6484–6496, Jul. 2021, doi: 10.1109/TVT.2021.3087036.
[24] J. Lin and Z. Yan, "An efficient list decoder architecture for polar codes," IEEE Trans. Circuits Syst. I, vol. 61, no. 6, pp. 1746–1754, Jun. 2014, doi: 10.1109/TCSI.2014.2299812.
[25] Y. Zhou, W. Song, and J. Yuan, "Fast-SSC-Flip decoding of polar codes," IEEE Commun. Lett., vol. 18, no. 11, pp. 1879–1882, Nov. 2014, doi: 10.1109/LCOMM.2014.2362751.
[26] S. A. Hashemi, C. Condo, and W. J. Gross, "Fast and flexible successive-cancellation list decoders for polar codes," IEEE Trans. Signal Process., vol. 65, no. 21, pp. 5756–5769, Nov. 2017, doi: 10.1109/TSP.2017.2734119.
[27] F. Ercan, T. Tonnellier, and W. J. Gross, "Energy-efficient hardware architectures for fast polar decoders," IEEE Trans. Circuits Syst. I, vol. 67, no. 1, pp. 163–175, Jan. 2020, doi: 10.1109/TCSI.2019.2936940.
[28] J. Choi, "On power allocation for uplink NOMA with SIC," IEEE Commun. Lett., vol. 20, no. 3, pp. 438–441, Mar. 2016, doi: 10.1109/LCOMM.2016.2518170.
[29] Y. Sun, D. W. K. Ng, Z. Ding, and R. Schober, "Optimal joint power allocation and user pairing for NOMA: Theory and application," IEEE Trans. Commun., vol. 65, no. 3, pp. 1077–1090, Mar. 2017, doi: 10.1109/TCOMM.2016.2632054.
[30] Y. Liu, Z. Qin, M. Elkashlan, Y. Gao, and L. Hanzo, "Non-orthogonal multiple access for massive IoT connectivity," IEEE Internet Things J., vol. 5, no. 3, pp. 2129–2144, Jun. 2018, doi: 10.1109/JIOT.2018.2791950.